Mechanics of Materials 169 (2022) 104295

Contents lists available at ScienceDirect

Mechanics of Materials

journal homepage: www.elsevier.com/locate/mecmat

Research paper

Ring Hoop Tension Test for yield strength estimation: Numerical analysis for a novel correlation method and applicability for mechanical testing of tubes and pipes☆

Jose Calaf-Chica *, Jorge Martínez-Peña, Pedro Miguel Bravo Díez, Mónica Preciado Calzada

Research Group of Material Science and Engineering (CIMa), University of Burgos, Avenida Cantabria s/n, E09006 Burgos, Spain

ARTICLE INFO

Keywords:
Small Ring Test
Ring Hoop Tension Test
Yield strength
Pipes
Tubes

ABSTRACT

The tubes and pipes manufacturing industry characterizes the mechanical properties of their products with a wide selection of standards, but most of them are qualitative testing methodologies. To estimate the mechanical properties from a quantitative point of view there are limited options in standards. In that sense, the standard tensile test is the preferred alternative by the manufacturers, but this option limits the mechanical estimation for the longitudinal direction of the tube–pipe product. Particular efforts have been made to design an alternative mechanical testing procedure to characterize the mechanical properties in the hoop direction of pipes and tubes. The Ring Hoop Tension Test (RHTT) was designed to fill this gap, but it shows limitations related to the required tooling and the influence of the frictional contact between the tooling and the ring specimen. In the nuclear industry, the Small Ring Test (SRT), a miniature test derivated from the RHTT, has been investigated in recent years. In this investigation, a novel RHTT was designed to overcome the limitations of SRT and RHTT, and a new procedure was implemented to estimate the yield strength of tubes and pipes. Numerical FEM simulations were performed to reach an optimum estimation method for the yield strength with the specific geometry of the SRT and a wide selection of pipe geometries with the RHTT. A set of hypothetical materials were designed to perform these analyses, taking into account the influence of Young's modulus, proportional limit, hardening coefficient (based on the Ramberg–Osgood law), and presence of Lüders bands straining. To verify the results obtained from this numerical FEM analysis, experimental tests (standard tensile tests and RHTTs) and metallographic analysis were performed on aluminum Al 6063 T6 and copper C12200 R360 tubes, showing the capability of this optimized RHTT to estimate the yield strength in the hoop direction for anisotropic tubes and pipes.

1. Introduction

Different challenges of the nuclear industry at the end of the seventies motivated the searching of alternatives to the standard tests for the characterization of radiation embrittlement (Manahan et al., 1981; Baik et al., 1983) and alteration of the yield strength (Zhong et al., 2020; Calaf-Chica et al., 2020), the ultimate tensile strength (Tantideeravit and Kamaya, 2020; Simonovski et al., 2018), the elongation at fracture (Kubík et al., 2018; Lee et al., 2021) and ductility of nuclear vessel materials. These novel testing methodologies had to comply with a singular specification: a miniature geometry. The sense of this requirement was based on the intrinsic limitations of the usable volume into the nuclear vessel, and the relationship between specimen volume and timing for radiation embrittlement. Nowadays research on miniature testing is mainly focused on the Small Punch Test (SPT; see Fig. 1(a)), but there are many other alternatives (Hiyoshi et al., 2020; Nozaki et al., 2020; Zheng et al., 2020), which show specific advantages and disadvantages in comparison with the SPT. This miniature test implies the use of a squared specimen of 10 × 10 × 0.5 mm or a circular specimen with a diameter higher than 8 mm and similar thickness (0.5 mm). The SPT specimen is clamped between two dies and punched until failure with a hardened steel ball of a diameter of 2.5 mm. Punch load versus punch displacement (SPT curve) is registered during the test. From the SPT curve, specific data are obtained depending on different methodologies, and the mechanical property is estimated by entering these data on the corresponding empirical correlation equation. The comparison between the stress field of a standard tensile test (mainly uniaxial) and the SPT

☆ This research did not receive any specific grant from funding agencies in the public, commercial, or not-for-profit sectors.
* Corresponding author.
E-mail addresses: jcalaf@ubu.es (J. Calaf-Chica), jmp0082@alu.ubu.es (J. Martínez-Peña), pmbravo@ubu.es (P.M. Bravo Díez), mpreciado@ubu.es (M. Preciado Calzada).

https://doi.org/10.1016/j.mechmat.2022.104295
Received 9 October 2021; Received in revised form 18 January 2022; Accepted 22 March 2022
Available online 29 March 2022

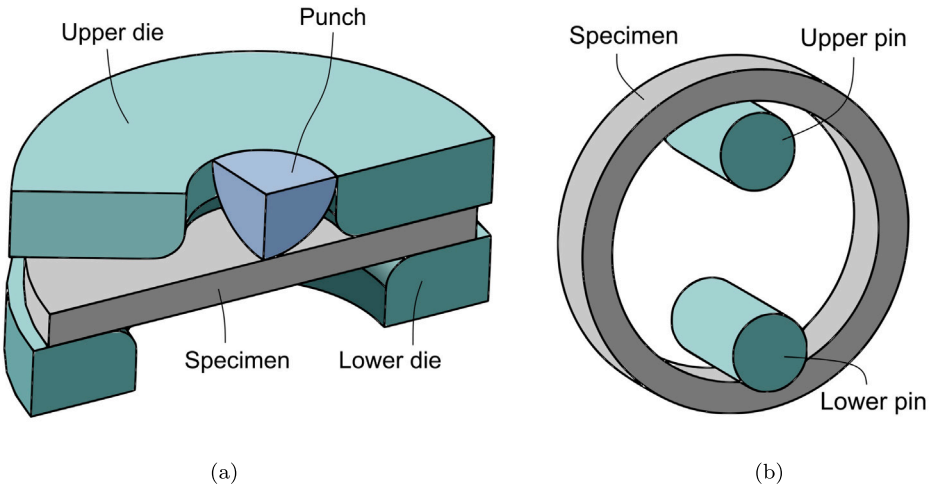

Fig. 1. (a) SPT set-up, (b) SRT set-up.

(mainly biaxial) is a clear sign of the inherent and high differences between both testing methodologies. This leads to moderate deviations in the mechanical property estimation by the SPT. This is the main reason that motivates the research of alternatives to the SPT and its tricky correlation methods. In that sense, Kazakeviciute et al. (2019) developed in 2019 a novel miniature technique for material stress–strain curve estimation: the Small Ring Test (SRT). The SRT specimen was a miniature ring with external and internal diameters of 11 mm and 9 mm respectively, and a width of 2 mm. This specimen is loaded with upper and lower high strength alloy pins of 2.5 mm in diameter (see Fig. 1(b)). Although this testing methodology is mainly dominated by bending stresses, the stress field is mostly uniaxial. Thus, at first sight, it seems that the SRT correlation with the standard tensile test should be more appropriate than SPT correlation. In a recent investigation of Rouse et al. (2020), the SRT was successfully used to estimate the alteration of mechanical properties along an additively manufactured volume of Ti-6Al-4V titanium alloy.

Although the SRT is a novel testing method in the field of miniature testing, the estimation of mechanical properties of specimens with a ring shape has extended research in the characterization of tubular forms (Ktari et al., 2021; Aghamiri et al., 2020; Garrison et al., 2021; Gurovich et al., 2020). Generally, the manufacturing process of tubular forms generates anisotropic microstructures. This makes it necessary to estimate mechanical properties in longitudinal and hoop directions. Tubes and pipes can be tested longitudinally with standard tensile tests (specified in ASTM E8 or ISO 6892), but it is difficult to define a reliable testing procedure similar to the tensile test in the hoop direction. The large curvature of the pipe in the hoop direction requires flattening the sample, but the forming process could lead to modifying the material properties.

Investigations published in the last decades regarding tube and pipe testing have been focused on two ways:

1. Qualitative testing procedures (see Fig. 2). They point to the loading capability of the pipe, without estimating any specific mechanical property. These methodologies are also known as technological tests. For the specific case of metallic tubular shapes: flattening test (ISO 8492 ISO/IEC, 2013a), ring tensile test (ISO 8496 ISO/IEC, 2013d), drift-expanding test (ISO 8493 ISO/IEC, 1998), flanging test (ISO 8494 ISO/IEC, 2013b) and ring-expanding test (ISO 8495 ISO/IEC, 2013c).
2. Quantitative testing procedures (see Fig. 3). In this type of test, one or more mechanical properties are estimated. Uniaxial tensile test (ASTM E8 ASTM, 2021 or ISO 6892 ISO/IEC, 2019) applies to the estimation of longitudinal mechanical properties, but there are not any standards for hoop properties estimation. This gap is filled by novel methodologies:
   (a) Tube expansion test (Kuwabara and Sugawara, 2013; Nazari Tiji et al., 2020; Korkolis et al., 2010). This is the ideal test for mechanical properties estimation in hoop direction, but the testing equipment is relatively complex and it requires a secure design conception.
   (b) Tube-end flaring test (Daxner et al., 2005; Jiang and Wang, 2018). This is the quantitative adaptation of the qualitative drift-expanding test (ISO 8493). Although this methodology is simple in its definition, friction between the flaring die and the pipe introduces biaxial stress fields in the specimen.
   (c) Ring Hoop Tension Test (RHTT) (Jiang et al., 2008; Dick and Korkolis, 2014b,a). This is the simplest methodology and it requires a minimum amount of material. Set-up is similar to the SRT designed by Kazakeviciute et al. but with differences in tooling and specimen geometries. There are set-ups with D-shaped pins with diameters equal to the inner diameter of the specimen. It results in no bending stresses during the test, but this methodology needs specific tooling for each ring geometry. A simpler set-up uses pins with a lower diameter. It expands their use to many ring geometries, but it introduces bending stresses in the specimen during the test. The influence of pins diameter in the test results generates an uncertainty that should be evaluated.

Within the quantitative testing procedures, researchers have shown notable interest and a significant publication rate in connection with the RHTT. This results from the fact that RHTT has simple geometries for tooling and specimen, and stress fields close to the standard tensile test. But comparing with the testing set-up of ISO 8496 or the design developed by Kazakeviciute et al. (2019), upper and lower D-shaped pins have ad-hoc geometries that depend on the specimen geometry. In that sense, ISO 8496 set-up is more flexible based on their small pins. Moreover, the RHTT is more sensitive to the variation of the friction coefficient between tooling and specimen, which is not the case for ISO 8496 set-up. This is why this investigation was focused on designing a methodology to estimate mechanical properties with the ISO 8496 set-up (a quantitative version of ISO 8496). Therefore, an extensive study of the set-up proposed by ISO 8496 and Kazakeviciute et al. (2019) was performed. A numerical analysis using the Finite Element Method (FEM) was developed to understand the behavior of the SRT specimen during testing. This analysis was extended to the influence of the mechanical properties and the tooling-specimen geometry on the load–displacement curve of the Ring Hoop Tensile Test with small pins. Finally, numerical results were validated with experimental tests on aluminum and copper tubes.

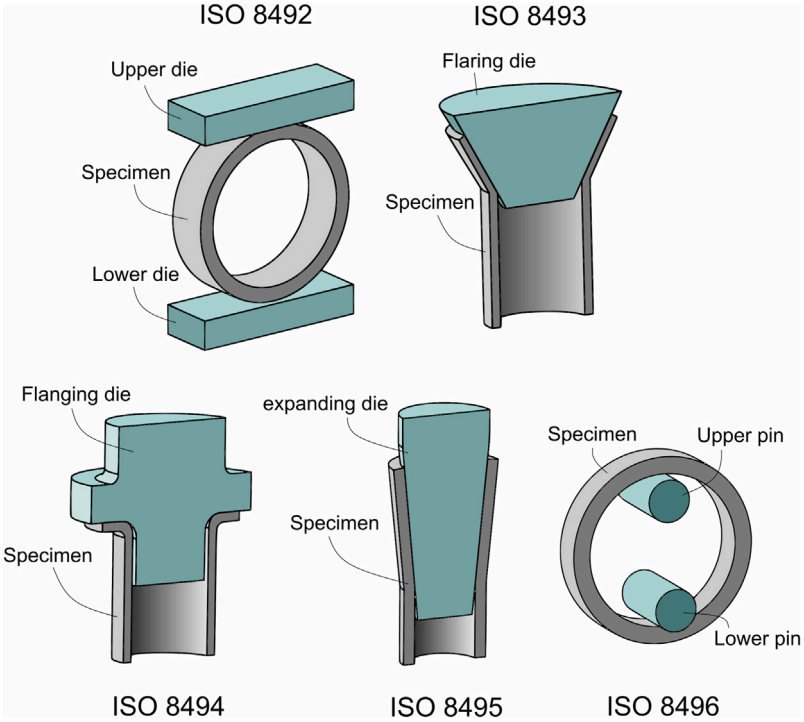

Fig. 2. Set-ups of qualitative testing procedures.

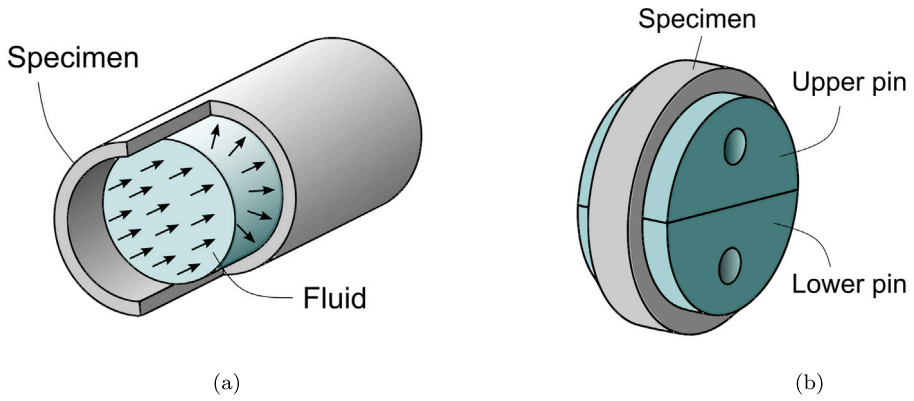

Fig. 3. Quantitative testing procedures: (a) Tube expansion test; (b) Ring Hoop Tension Test.

2. Materials and methods

As mentioned in the Introduction section, numerical FEM analyses and experimental tests were performed to design and validate a methodology to estimate the yield strength of metallic thin-thickness tubes and pipes with the set-up of SRT. This study was divided into two sections or parts: (WP1), designing of an estimation methodology for the specific specimen geometry of the SRT, and, (WP2), an extension of this proposed procedure to other specimen geometries (alteration of outer/inner diameters and width of the specimen), to design a versatile testing procedure for thin tubes and pipes.

2.1. Estimation of the yield strength with the SRT (WP1)

Simulations of the SRT were performed with ANSYS Mechanical 2021 R1 software. As mentioned previously, the geometry of the SRT specimen was outer/inner diameters of 11/9 mm and a width of 2 mm. Upper and lower pins had a diameter of 2.5 mm. A 3D model was designed considering the three symmetries of the SRT to reduce the computing cost (see red faces of Fig. 4(a)). Meshing used quadratic hexahedral elements and a minimum of 5 elements throughout part thicknesses (see Fig. 4(b)). Pin-specimen contact was established with Augmented Lagrange formulation and a frictional coefficient of $\mu = 0.1$, although a sensibility analysis for μ value was included in the simulation set.

Isotropic linear elastic model and multilinear isotropic hardening model were used to simulate the elastic–plastic behavior of the specimen material. A Ramberg–Osgood power law was applied following Eq. (1) for the plastic behavior.

$$\epsilon_p = K\left[\left(\frac{\sigma}{\sigma_p}\right)^n - 1\right] \tag{1}$$

where: K and n are the hardening coefficients, σ is the true stress, ϵ_p is the plastic strain, and σ_p is the proportional limit.

Twelve hypothetical materials were implemented (see Table 1) in the SRT simulations in order to analyze the influence of each mechanical property in the load–displacement curve of the SRT. Pins were simulated with a pure isotropic linear elastic model (see properties in Table 1). Considering that material data for simulations needs the stress limit between the elastic and plastic behavior (proportional limit)

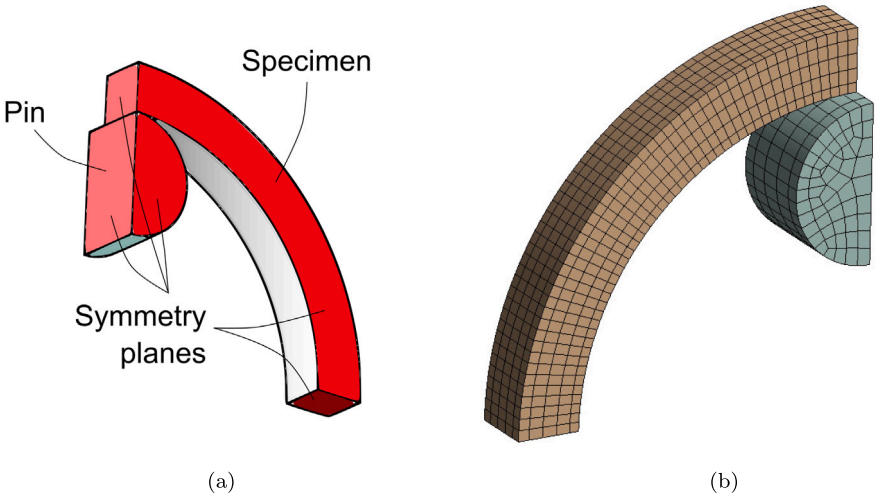

Fig. 4. 3D FEM model of the SRT (WP1): (a) Geometry; (b) Meshing. (For interpretation of the references to color in this figure legend, the reader is referred to the web version of this article.)

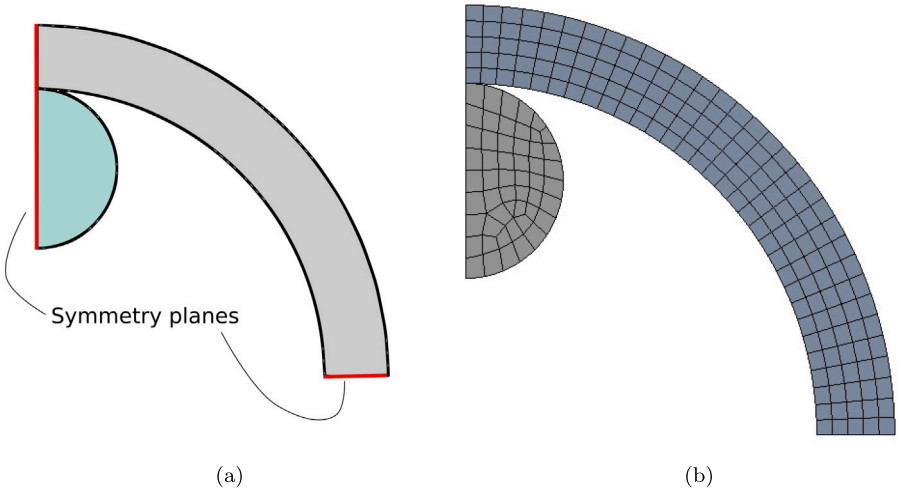

Fig. 5. 2D FEM model of WP2: (a) Geometry; (b) Meshing.

Table 1
Mechanical properties of the hypothetical materials (WP1).

ID	E (GPa)	ν	σ_p (MPa)	n	σ_y (MPa)
Pin material	200	0.3	N/A	N/A	N/A
WP1-HM1	200	0.3	200	5	229.7
WP1-HM2	200	0.3	200	10	214.4
WP1-HM3	200	0.3	200	30	204.7
WP1-HM4	200	0.3	500	5	574.3
WP1-HM5	200	0.3	500	10	535.9
WP1-HM6	200	0.3	500	30	511.7
WP1-HM7	200	0.3	1000	5	1148.7
WP1-HM8	200	0.3	1000	10	1071.8
WP1-HM9	200	0.3	1000	30	1023.4
WP1-HM10	150	0.3	200	10	214.4
WP1-HM11	100	0.3	200	10	214.4
WP1-HM12	50	0.3	200	10	214.4

and not the yield strength (which considers an offset strain), Table 1 includes the calculation of the yield strength (using an offset strain of $K = 0.002$), based on the hardening law used in the simulations.

In order to evaluate the influence of the friction coefficient μ in the SRT, WP1-HM1 material was also simulated with a higher μ value ($\mu = 0.3$).

From these simulations, load–displacement curves (SRT curves) were registered, and a detailed analysis was performed to understand the relationship between the SRT curves and stress–strain fields in the specimen. From this analysis, a methodology to estimate the yield strength with the SRT curve was established.

2.2. Methodology extension to other specimen geometries (WP2)

The applicability of the SRT is limited to a specific tooling-specimen geometry. To extend this testing method to the estimation of hoop yield strength of seamless tubing and pipes, a second study (WP2) was performed analyzing the influence of geometry parameters on the results obtained in WP1. A systematic FEM analysis was carried out considering the following specimen input data: slenderness ratio ($D_{ext}/t = [11, 20, 30, 40]$), thickness ($t = [0.5, 1.0, 2.0]$ mm), and width ($w = 1.0$ mm). To reduce the computational cost of this numerical analysis, geometry was simplified to a 2D model (see Fig. 5). Plane stress formulation was considered based on the non-significant constraining along the specimen width direction. Table 2 shows the hypothetical materials designed for these simulations, and Table 3 includes all the geometry combinations, resulting in 96 simulations. To validate the use of a simplified 2D model, two similar materials (ID WP1-HM9 and ID

Table 2
Mechanical properties of the hypothetical materials (WP2).

ID	E (GPa)	ν	σ_p (MPa)	n	σ_y (MPa)
WP2-HM1	50	0.3	50	5	57.4
WP2-HM2	50	0.3	50	30	51.2
WP2-HM3	50	0.3	500	5	574.3
WP2-HM4	50	0.3	500	30	511.3
WP2-HM5	200	0.3	100	5	114.9
WP2-HM6	200	0.3	100	30	102.3
WP2-HM7	200	0.3	1000	5	1148.7
WP2-HM8	200	0.3	1000	30	1023.4

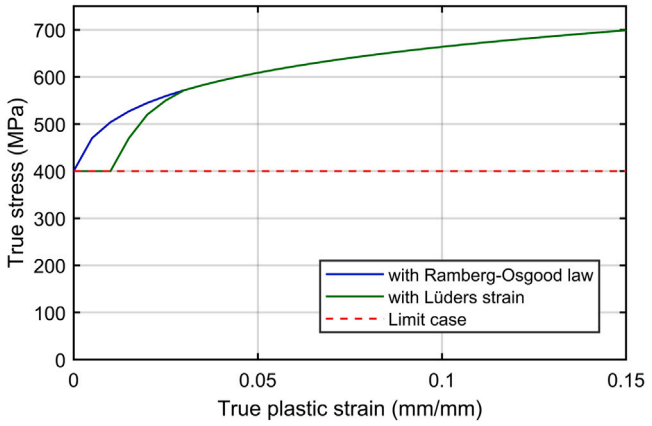

Fig. 6. Stress–plastic strain curves used in the analysis of the Lüders bands influence.

WP2-HM8) were compared with a 3D model and two 2D models, one with plane stress elements and another one with plane strain elements.

In a final FEM analysis, the presence of Lüders bands straining and its influence in the yield strength estimation procedure with the RHTT was analyzed. A singular hypothetical material WP2-HM9 was designed with E = 200 GPa, ν = 0.3 and σ_p = 400 MPa, and three derivatives for plastic behavior: with a Ramberg–Osgood law (n = 7.7), with a Lüders strain of 0.01 mm/mm and subsequent hardening similar to the previous one, and a limit case with an infinite Lüders strain, which is equivalent to the use of a Ramberg–Osgood law with $n = \infty$. Fig. 6 shows the stress–plastic strain curves used in this FEM analysis, which used the geometry case WP2-G40-20.

3. Results and discussion

3.1. Estimation of the yield strength with the SRT (WP1)

Fig. 7 shows the load–displacement curves (SRT curves) of the hypothetical materials with similar Young's modulus (E = 200 GPa). The first zone of the SRT curves and its slope were common for all of these materials, indicating that its initial pure elastic behavior was in a direct link with the elastic modulus. Each set of colored curves indicated three hypothetical materials with similar proportional limit σ_p but different strain-hardening coefficient n. Thus, the more strain-hardening capability had the material (low n), the higher SRT curve slope was. Changes in curve color but similar curve format (solid, dashed or dashed-dotted line) meant changes only in proportional limit. As a result, an increment in the proportional limit extended the elastic initial zone of the SRT curve and increased the slope of the plastic zone of the SRT curve. There was a clear limit between the elastic and plastic zones, similar to the standard tensile test. This is confirmed in Fig. 8, where the curves represent the hypothetical materials WP1-HM2, WP1-HM10, WP1-HM11 and WP1-HM12 which have a similar proportional limit and hardening coefficient and dissimilar Young's modulus. It means that the elastic response of the rings should be

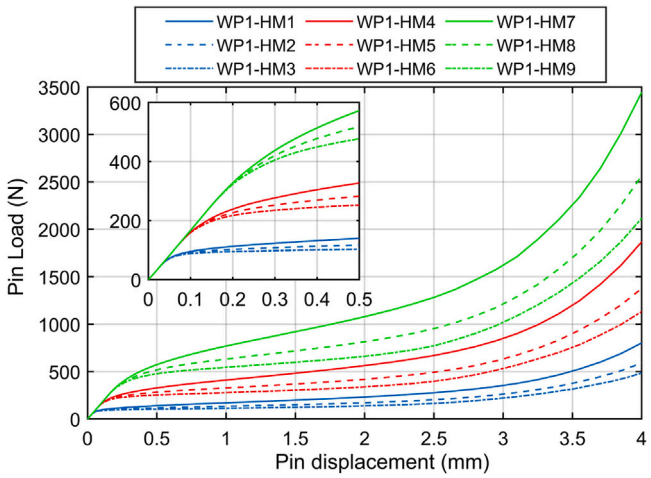

Fig. 7. Load–displacement curves (SRT curves) for the hypothetical materials HM1 to HM9 (WP1). (For interpretation of the references to color in this figure legend, the reader is referred to the web version of this article.)

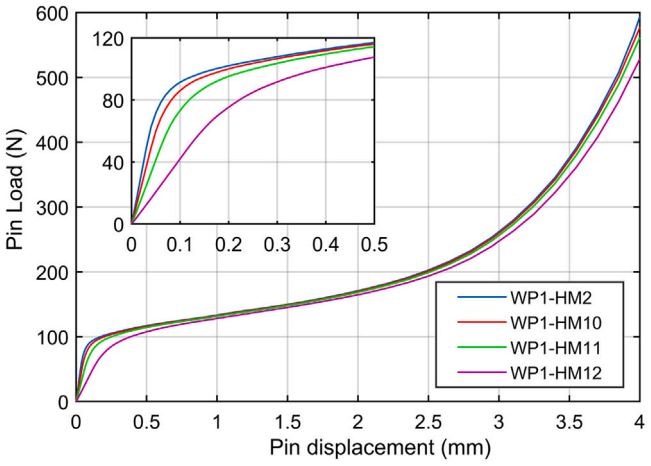

Fig. 8. SRT curves for the hypothetical materials HM2 and HM10 to HM12 (WP1).

dissimilar and the plastic behavior should show overlapped in the load–displacements curves, and Fig. 8 confirmed this assumption: curves show dissimilar behavior in the first stages of the test and similar behavior after a specific pins displacement. It shows the clear transition between elastic and plastic zones in the SRT curve. In addition, changes in Young's modulus motivate changes in the initial slope of the elastic zone (see Fig. 8). It means that this initial slope is sensitive to Young's modulus and insensitive to the plastic properties. Thus, the initial slope of the SRT curve could be correlated with Young's modulus of the ring material.

Fig. 9 shows the Von Mises stress and the plastic strain at the end of the initial straight zone of the SRT curve for the hypothetical material WP1-HM4 (approx. 0.1 mm, see Fig. 7). The maximum plastic strain of 0.0026 and the non-significant yielded volume are signals of dominant elastic behavior. Von Mises stress just in the pin-ring contact that is close to the proportional limit (σ_p = 500 MPa) shows that the ring is in the proximity of the transition between the pure elastic behavior and the elastic–plastic behavior. Thus, the first zone of the SRT curve is driven by the elastic properties, and just when the slope of the SRT curve decreases, the plastic properties come into play. This is another evidence of the clear elastic–plastic transition in the SRT curve.

Fig. 10 shows the correlation between the initial slope of the SRT curves ($Slope_{ini}$) and the Young's modulus of the hypothetical materials. The linear least squares method showed good R^2 values for

Table 3
Geometry data for WP2 FEM simulations.

ID	D_{outer}/t	t (mm)	w (mm)	ID	D_{outer}/t	t (mm)	w (mm)
WP2-G11.05	11	0.5	1.0	WP2-G30.05	30	0.5	1.0
WP2-G11.10	11	1.0	1.0	WP2-G30.10	30	1.0	1.0
WP2-G11.20	11	2.0	1.0	WP2-G30.20	30	2.0	1.0
WP2-G20.05	20	0.5	1.0	WP2-G40.05	40	0.5	1.0
WP2-G20.10	20	1.0	1.0	WP2-G40.10	40	1.0	1.0
WP2-G20.20	20	2.0	1.0	WP2-G40.20	40	2.0	1.0

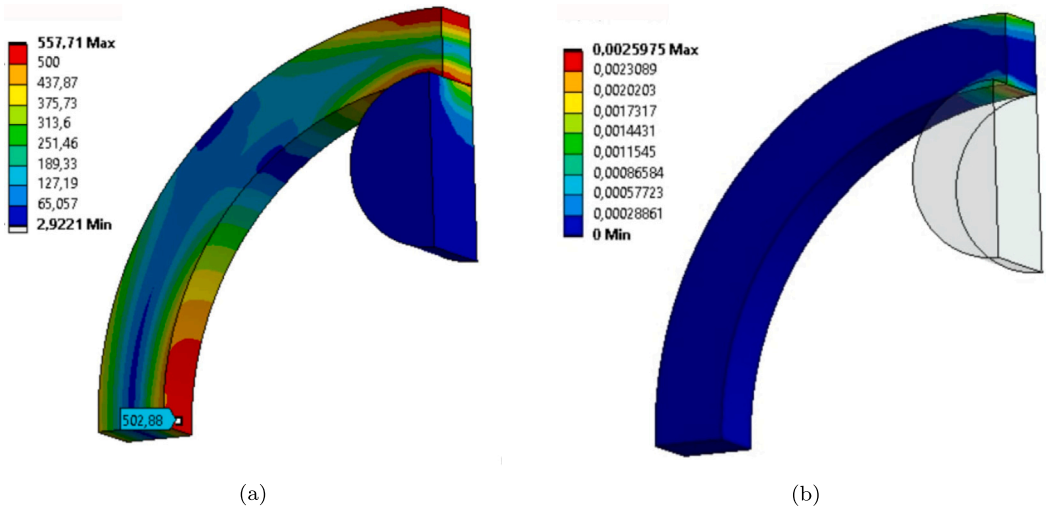

Fig. 9. (a) Von Mises stress and (b) plastic strain at the end of the initial straight zone of the SRT curve for hypothetical material WP1-HM4.

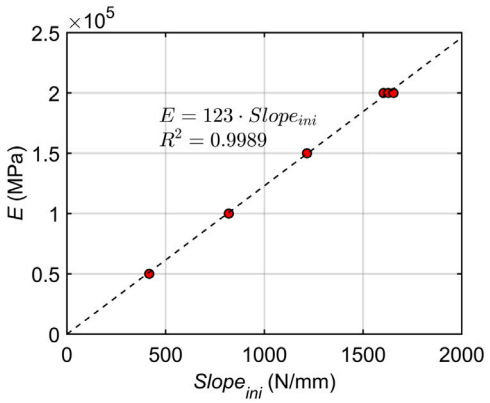

Fig. 10. Correlation of $Slope_{ini}$ and Young's modulus.

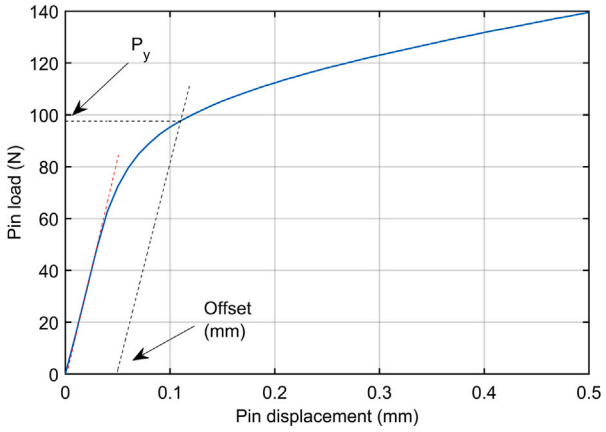

Fig. 11. Offset methodology for the yield strength estimation with the SRT.

this relationship, verifying the previous assumptions and obtaining the correlation Eq. (2) for the Young's modulus estimation with the SRT. Thus, the SRT estimates the Young's modulus in the same way that is performed in the uniaxial tensile test.

$$E = 123 \cdot Slope_{ini} \tag{2}$$

Similarities between the initial stages of the SRT curve and the stress–strain curve of a tensile test suggested the use of a similar procedure to estimate the yield strength with the SRT specimen. Following the methodology of a standard tensile test, a yield load P_y was obtained from the crossing point between an offset line, parallel to the tangent line to the $Slope_{ini}$, and the SRT curve (see Fig. 11). Two variables should be fixed in order to use this offset procedure: firstly, the offset value; and secondly, the morphology of the correlation equation that relates the yield strength with the yield load ($\sigma_y = f\left(P_y\right)$).

Fig. 12 shows the correlation between the yield strength and the yield load for an offset of 0.05 mm and simulations performed in WP1. This followed a linear correlation by Eq. (3) with a correlation coefficient $\alpha = 2.548$ mm^{-2} and $R^2 = 0.9974$.

$$\sigma_y = 2.548 \cdot P_y \tag{3}$$

A wide range of offset values was used to calculate the α_i coefficient per each i material of Table 1. A mean value $\bar{\alpha}$ (Eq. (4)) and a standard deviation σ (Eq. (5)) were calculated per each offset, searching for the offset value which showed the minimum deviation. Fig. 13 represents the mean value $\bar{\alpha}$ and the standard deviation σ per each offset, obtaining the minimum deviation for a value of $\bar{\alpha} = 2.136$ mm^{-2} with an offset = 0.15 mm. Table 4 shows the estimated yield strength with the simulations of the SRT and using Eq. (6) and an offset =

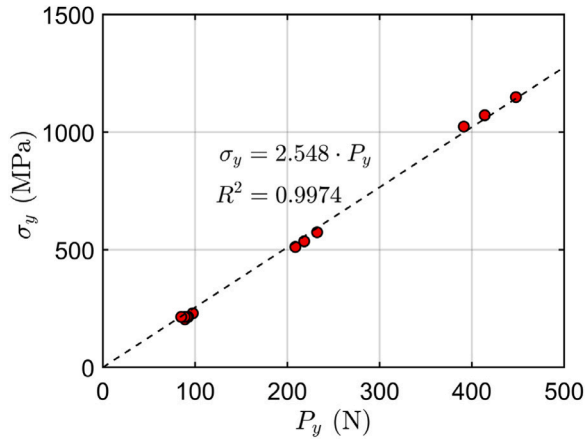

Fig. 12. Correlation of P_y and yield strength (materials WP1; Offset = 0.05 mm).

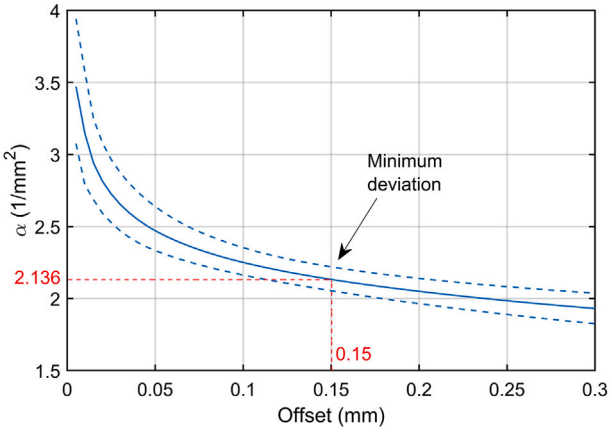

Fig. 13. Correlation coefficient α (mean value: solid line; deviation: dashed line) versus offset value.

Table 4
Estimated yield strength for offset = 0.15 mm and $\alpha = 2.136$ mm^{-2}.

ID	σ_y real (MPa)	P_y (N)	σ_y estimated (MPa)	Error (%)
WP1-HM1	229.7	114.7	245.0	6.6
WP1-HM2	214.4	102.9	219.7	2.5
WP1-HM3	204.7	95.1	203.1	−0.8
WP1-HM4	574.3	282.0	602.4	4.9
WP1-HM5	535.9	252.2	538.7	0.5
WP1-HM6	511.7	233.2	498.1	−2.6
WP1-HM7	1148.7	560.2	1196.5	4.2
WP1-HM8	1071.8	494.5	1056.3	−1.4
WP1-HM9	1023.4	454.1	969.9	−5.2
WP1-HM10	214.4	102.5	218.9	2.1
WP1-HM11	214.4	101.4	216.7	1.1
WP1-HM12	214.4	99.9	213.4	−0.4

0.15 mm.

$$\bar{\alpha} = \frac{\sum_{i=1}^{12} \alpha_i}{12} \tag{4}$$

$$\sigma = \sqrt{\frac{\sum_{i=1}^{12} (\alpha_i - \bar{\alpha})^2}{12}} \tag{5}$$

$$\sigma_y = 2.136 \cdot P_y \tag{6}$$

As mentioned in the methodology section, FEM simulations of the SRT for the hypothetical material WP1-HM1 were performed with two different values of the friction coefficient μ, $\mu = (0.1, 0.3)$, for the contact between pins and ring. Fig. 14(a) shows the comparison between both simulations, where SRT showed no significant sensibility to the friction coefficient. The sense of this behavior was based on the small contact surface between pins and ring during most of the test (see Fig. 14(b)). Small contact surface means small affected ring volume to constraining due to contact sticking (high friction coefficient) or free sliding (small friction coefficient), and small affected ring volume means small alterations in the load–displacement curve.

3.2. Methodology extension to other specimen geometries (WP2)

The aim of WP2 was the obtaining of a correlation equation to the estimation of the yield strength with the RHTT (Ring Hoop Tension Test) considering the influence of ring geometry. This WP2 was based on 96 FEM simulations of the RHTT with different geometries and hypothetical materials. In order to reduce the computational cost of this analysis, a simplified 2D FEM model was used instead of the 3D FEM model of WP1. Before the systematic launching of these simulations, a comparison was done between results obtained from both models for similar geometrical and material data. Fig. 15 represents three RHTT curves for the ring geometry of SRT (ID WP2-G11.05 of Table 3 with w = 2.0 mm) and material ID WP2-HM8 (see Table 2). Similarity between RHTT curves for 3D FEM model and 2D plane stress FEM model validated the use of the simplified 2D plain stress model for the WP2 analysis. The reason for the similarity of the plane stress 2D model and the 3D model was based on: (i) the absence of any restriction (boundary condition) to through-width deformation of the ring during the test, and (ii) the uniform circumferential deformation along the width direction of the ring. These two facts ensured the absence of any significant stress along the ring width compared with the circumferential stress.

The RHTT considered in this investigation used pins diameters lower than the inner diameter of the ring. To reduce the complexity of RHTT tooling, the set of pin diameters needed for testing a variety of ring geometries should be kept to a minimum quantity. Thus, the sensitivity of RHTT curve to the pin diameter should be non-significant. Fig. 16(a) shows the RHTT curve for material ID WP2-HM8 and geometry ID WP2-G40.20 with two pin diameters: 10 mm and 21 mm. RHTT curves followed similar shape until a pin displacement of around 10 mm. Thus, if the crossing point obtained from the offset method had a pin displacement lower than 10 mm, similar yield load P_y would be obtained, and pin diameter would not influence the yield strength estimation. This transition between similar load–displacement curve to dissimilar curve is based on the deformation stages of the RHTT. This ring test is a bending test that is gradually transformed to a uniaxial tensile test (see Fig. 16(b)). Bending stiffness of the non-deformed ring is much smaller than uniaxial tensile stiffness in the final steps of the RHTT. Thus, transition between both scenarios corresponds with the exponential increment of the slope in the load–displacement curve of the test. The necessary pins displacement to reach the uniaxial tensile behavior has dependency with the pin diameter: big pins shorten the required pin displacement and small pins extend this pin displacement to reach the bending-tensile transition. Before this transition, pin diameter does not influence in the load–displacement curve because the contact surface does not show significant changes from one pin to another.

Following similar analysis steps of WP1 for each WP2 geometry (see IDs in Table 3), different offset values were used to obtain the correlation coefficients α_i per each hypothetical material (see Table 2). A mean value $\bar{\alpha}$ (Eq. (4)) and a standard deviation σ (Eq. (5)) were calculated per each offset and WP2 geometry. Offset that showed the minimum α deviation was selected and appointed to the Table 5.

Fig. 17 represents the offset values (red dots) registered in Table 5 in correlation to the geometrical data (slenderness ratio D_{ext}/t and thickness t). Eq. (7) was obtained with a non-linear least squares method based on a polynomial surface fitting. Mesh surface plotted in

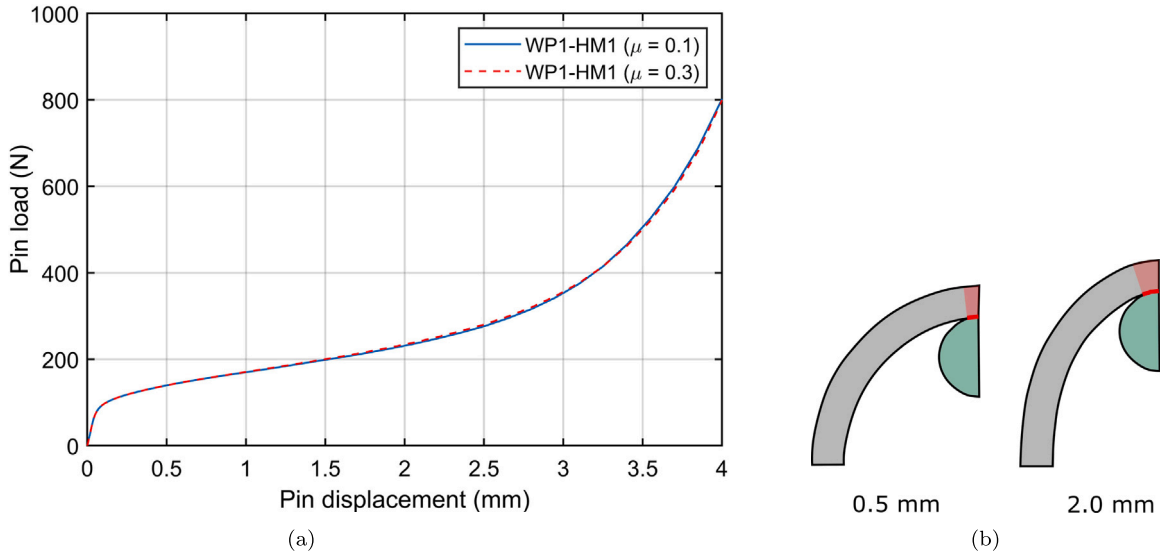

Fig. 14. (a) SRT curves for material WP1-HM1 with two different friction coefficients; (b) contact surface and affected ring volume due to sticking–sliding behavior.

Table 5
Offsets resulted from the WP2 simulations.

ID	Offset (mm)	$\bar{\alpha} \pm \sigma$ (mm^{-2})	ID	Offset (mm)	$\bar{\alpha} \pm \sigma$ (mm^{-2})
WP2-G11.05	0.050	9.51 ± 0.58	WP2-G30.05	0.240	28.5 ± 1.95
WP2-G11.10	0.100	4.76 ± 0.29	WP2-G30.10	0.485	14.2 ± 0.98
WP2-G11.20	0.185	2.39 ± 0.13	WP2-G30.20	0.895	7.16 ± 0.46
WP2-G20.05	0.140	18.2 ± 1.11	WP2-G40.05	0.375	38.7 ± 3.27
WP2-G20.10	0.305	8.98 ± 0.56	WP2-G40.10	0.745	19.4 ± 1.64
WP2-G20.20	0.590	4.49 ± 0.26	WP2-G40.20	1.380	9.75 ± 0.80

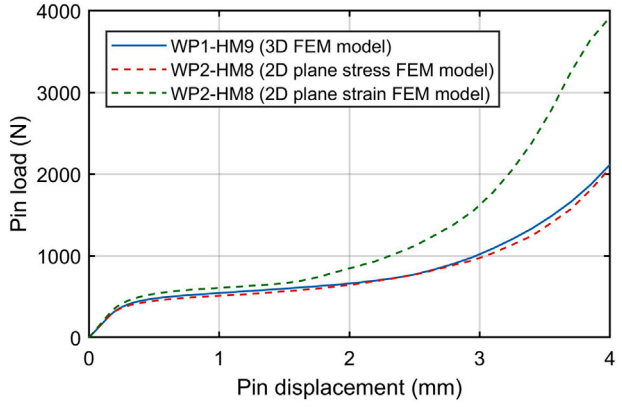

Fig. 15. Comparison between RHTT curves of 3D and 2D FEM models for geometry ID WP2-G11.05 with w = 2.0 mm.

Fig. 17 represents this correlation. The R^2 = 0.9934 obtained by this fitting procedure showed the goodness of Eq. (7).

$$\text{offset} = t\left(0.0205\frac{D_{ext}}{t} - 0.13\right) \tag{7}$$

The yield load P_y of each WP2 geometry and WP2 material was calculated using the offset deduced from Eq. (7). Correlation coefficients α were deduced from $\alpha = \sigma_y/P_y$, and Fig. 18 shows the correlation of α with ring slenderness D_{ext}/t and ring thickness t. Mesh surface plotted in Fig. 18 represents the non-linear least squares polynomial surface fitting that leads to Eq. (8) with R^2 = 0.9837. All these FEM simulations were done with a ring width of w = 1.0 mm. Thus, dependency of α with w was introduced in Eq. (8).

$$\alpha = \frac{\sigma_y}{P_y} = \frac{0.5054}{t \cdot w}\left(\frac{D_{ext}}{t} - 1.789\right) \tag{8}$$

The yield strengths of the hypothetical materials of WP2 were estimated using Eq. (8), and were compared with the real yield strength introduced in the simulations. Fig. 19 shows the estimation error (see Eq. (9)) in a histogram bar plot, where a negative skewness is shown in the frequency distribution. Nonetheless, for most cases, the estimation error of the yield strength was between ± 10%. This was a good result considering the wide selection of mechanical properties introduced in the WP2 simulations.

$$\text{error}(\%) = \left(\frac{\sigma_y^{\text{estimated}} - \sigma_y^{\text{real}}}{\sigma_y^{\text{real}}}\right) \times 100 \tag{9}$$

Fig. 20 shows the RHTT curves for the Lüders bands FEM analysis, where three hypothetical materials with different Lüders straining were used. Considering the selected geometry (ID WP2-G40.20), and using the Eqs. (7) and (8), the offset was equal to 1.38 mm and the correlation coefficient was α = 9.656 mm^{-2}. Table 6 shows the yield loads P_y obtained from the RHTT curves, and the estimated yield strengths. These estimated yield strengths should be compared with the real yield strengths that would be estimated from the stress–strain curves with the rules included in standards of the uniaxial tensile test (ASTM E8 ASTM (2021) or ISO 6892 ISO/IEC (2019)). Table 6 includes the use of ISO 6892 for the calculation of the real yield strengths of each hypothetical material and the error of the estimation procedure with the RHTT. The maximum error that was generated by the presence of Lüders straining was equal to 4.9%.

Experimental tests were performed in order to validate the correlation equations deduced numerically in this investigation. Two pipes of aluminum alloy 6063 T6 and copper alloy C12200 R360 were tested with tensile tubular specimens following the standard ISO 6892 and RHTT specimens with the ring geometry included in Table 7.

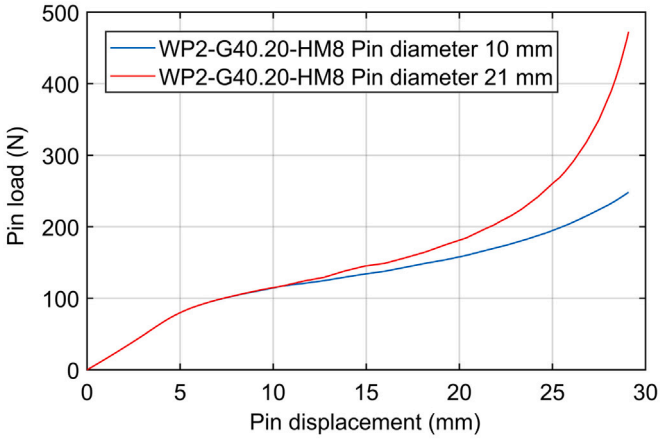

(a)

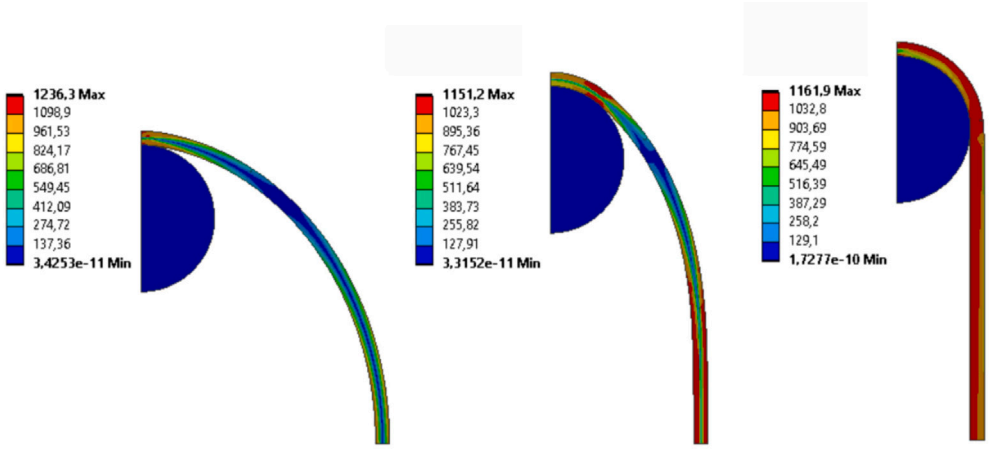

(b)

Fig. 16. (a) Comparison between RHTT curves of material ID WP2-HM8 and geometry ID WP2-G40.20 with two pin diameters: 10 mm and 21 mm, and (b) Von Mises stresses for different pins displacements (pin diameter of 21 mm).

Table 6
Parameters obtained from RHTTs of the Lüders bands influence analysis and yield strength estimation.

Material	Real σ_y (MPa)	P_y (N)	Estimated σ_y (MPa)	Error (%)
With Ramberg–Osgood law	437.4	45.9	443.2	1.3
With Lüders strain	400	41.3	398.8	0.3
Limit case	400	39.4	380.4	4.9

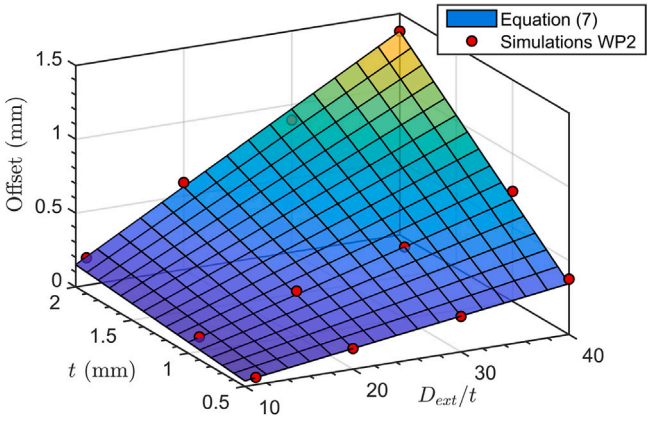

Fig. 17. Offset in correlation to ring slenderness and ring thickness.

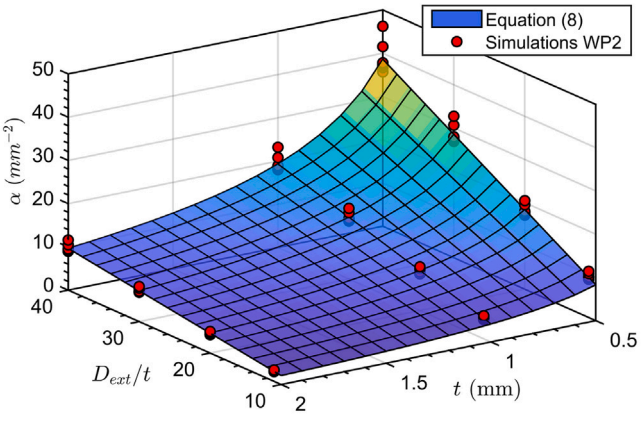

Fig. 18. α in correlation to ring slenderness and ring thickness.

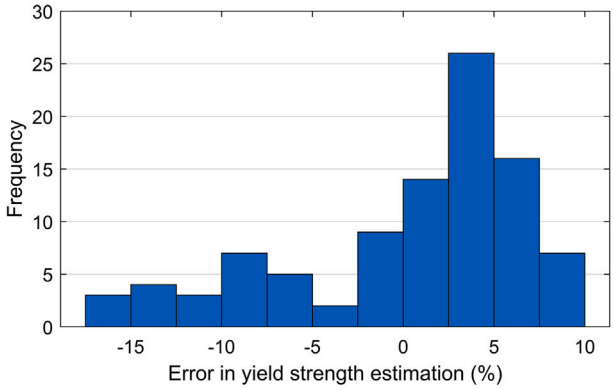

Fig. 19. Histogram of error in the estimation of the yield strength of WP2 simulations.

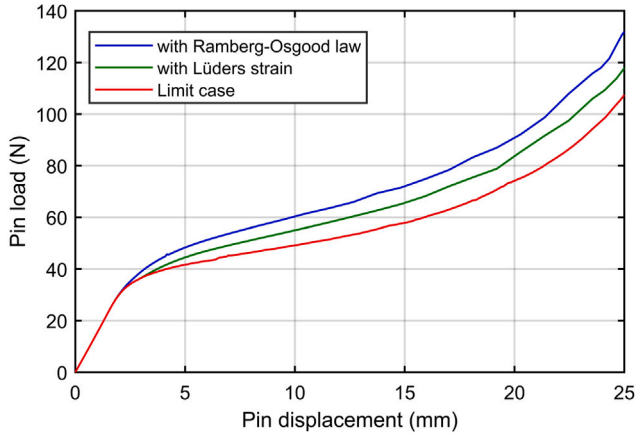

Fig. 20. RHTT curves of the Lüders bands influence analysis.

Table 7
Geometry of experimental RHTT.

Material	D_{ext}/t	t (mm)	w (mm)
Al 6063 T6	21.46	0.92	4.00
Cu C12200 R360	25.88	0.85	4.00

Experimental RHTT set-up used pins of stainless steel of diameter 6.0 mm and tooling to guarantee the self-alignment of the ring-pin contact during testing (see Fig. 21(a)). Displacement measurement in RHTT was done with the crosshead displacement signal of a universal testing machine. In order to eliminate the contribution derived from tooling and pins deformation, a calibration test was performed. The set-up for the calibration test consisted of crossed pins in contact with a circular disc plate of high-strength steel with a thickness of 2 mm (see Fig. 21(b)). Fig. 22 shows the calibration curve.

Fig. 23 represents the engineering stress–strain curves of the experimental materials obtained from standard tensile tests in the longitudinal direction of the pipes. Table 8 includes the mechanical properties estimated from these tests. It should be pointed out that mechanical properties obtained for Al 6063 T6 matched with values included in ASM Handbook for aluminum alloys (ASM International, 2019). Thus, non-significant strengthening by cold-working was expected in the manufacturing process of this pipe, as a sign of isotropic properties. This conclusion was supported by metallographies of transversal and longitudinal sections of the pipe (see Fig. 24), where isotropic grain structure denoted another sign of isotropic properties. By contrast, copper alloy metallurgical state R360 indicates an extremely cold-hardened material. The tensile test of C12200 pipe is coherent with this metallurgical state ID, showing extremely low elongation and

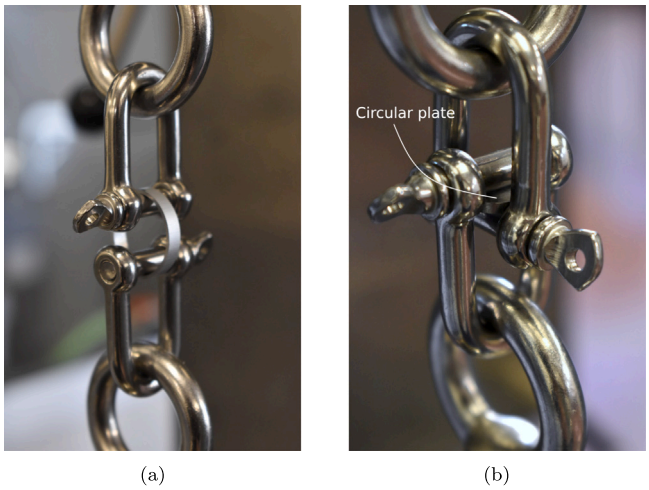

Fig. 21. (a) Experimental RHTT set-up; (b) Calibration test of RHTT.

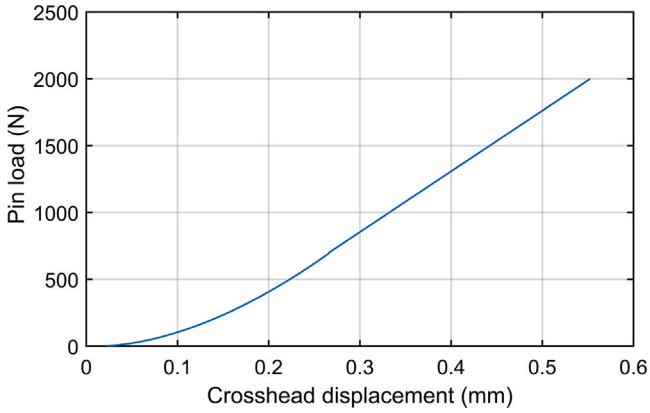

Fig. 22. Calibration test of the RHTT.

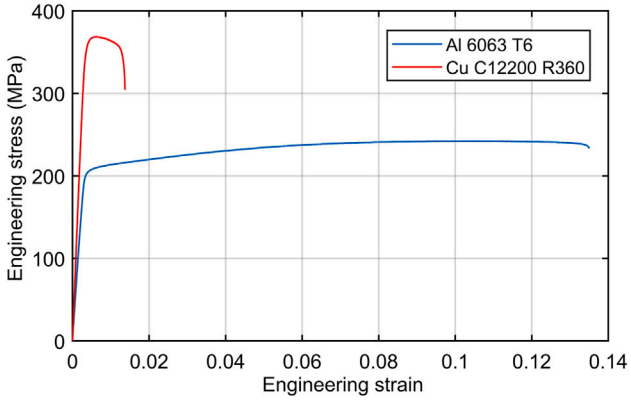

Fig. 23. Engineering stress–strain curves for tube tensile tests.

strain-hardening. Fig. 25 shows metallographies of transversal and longitudinal sections for this copper alloy, confirming an anisotropic grain structure.

Fig. 26 shows the RHTT curves registered for ring specimens of both aluminum and copper pipes. Using the Eqs. (7) and (8), yield strengths were estimated with offsets and P_y obtained from RHTT curves of Fig. 26. Table 9 includes the estimated yield strengths and the error which is calculated in the comparison with the mechanical properties deduced from tensile tests. Yield strength was similar in

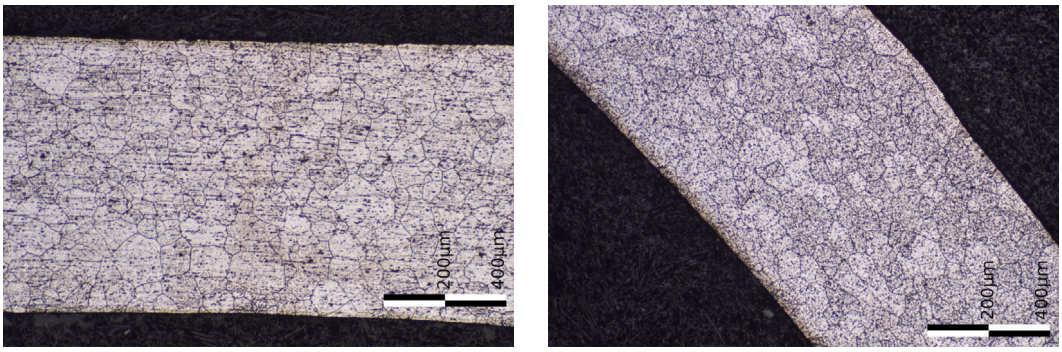

Fig. 24. Metallographies of Al 6063 T6 (Keller's etchant): (a) longitudinal section; (b) transversal section.

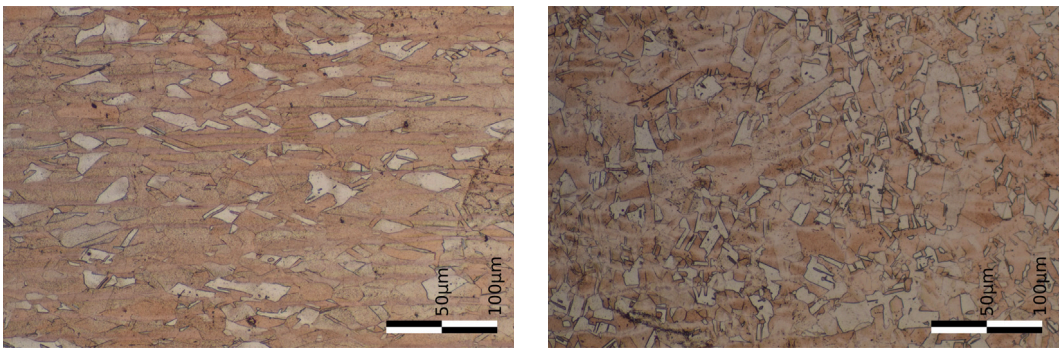

Fig. 25. Metallographies of Cu C12200 R360 (etchant: distilled water and nitric acid; 25 ml and 25 ml): (a) longitudinal section; (b) transversal section.

Table 8
Mechanical properties obtained from tensile tests.

Material	E (GPa)	σ_y (MPa)	σ_u (MPa)
Al 6063 T6	69.5	208.8	241.5
Cu C12200 R360	117.0	367.5	368.5

Table 9
Parameters obtained from experimental RHTTs and yield strength estimation.

Material	Offset (mm)	P_y (N)	σ_y estimated (MPa)	Error (%)
Al 6063 T6	0.285	77.65	209.8	0.5
Cu C12200 R360	0.340	89.10	319.1	−13.2

Table 10
Mechanical properties obtained from tube tensile tests.

Material	E (GPa)	σ_y (MPa)	σ_u (MPa)
Cu C12200 R360	117.0	367.5	368.5
Cu C12200 R360 + Annealing	117.0	285.0	305.8

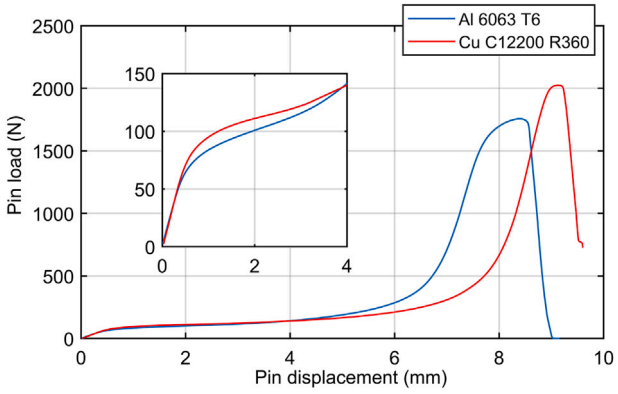

Fig. 26. RHTT experimental curves.

the case of aluminum pipe. This is coherent with the isotropic grain structure and mechanical properties obtained by tensile tests for this aluminum series and heat treatment. In the case of copper pipe, the estimated yield strength by RHTT was 13.2% lower than the obtained value by tensile testing. This difference could be originated by the anisotropic behavior assumed by its cold-formed metallurgical state and anisotropic grain structure. In that sense, the RHTT showed the lower mechanical capabilities of this copper pipe in the hoop direction.

To confirm the assumptions related to the differences found between longitudinal yield strength obtained from the tensile test and hoop yield strength estimated from RHTT for the copper pipe, an annealing treatment of 400 °C and 1 h was applied to soften the material, reducing the cold-working strengthening and its anisotropic behavior. Fig. 27 shows the metallographies of transversal and longitudinal sections of the copper pipe after the annealing process. The longitudinal section showed less directionality in the grain morphology, a sign of less anisotropy. Fig. 28(a) is a comparison of tensile tests for the as-received copper pipe and the annealed one. This testing verified the softening of the material after the annealing treatment, motivating the reduction of anisotropic behavior. Table 10 shows the mechanical properties deduced from the tensile tests. Fig. 28(b) represents the RHTTs for both as-received and annealed copper pipes. Eqs. (7) and (8) were applied to obtain the offset, P_y, and estimated yield strength for the annealed condition. Table 11 includes the mentioned RHTT parameters and correlation results. The annealed ring specimen showed an estimated hoop yield strength virtually identical to the resulted value in the longitudinal tensile test.

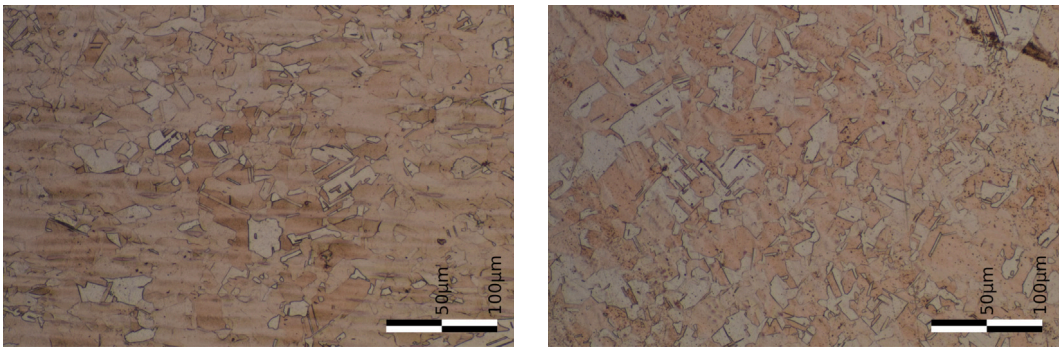

Fig. 27. Metallographies of Cu C12200 R360 after annealing at 400 °C and 1 h (etchant: distilled water and nitric acid; 25 ml and 25 ml): (a) longitudinal section; (b) transversal section.

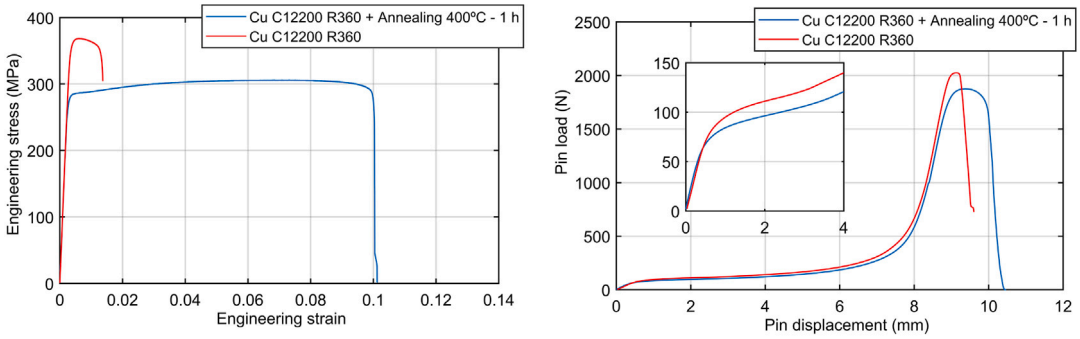

Fig. 28. Cu C12200 R360 pipe, as received and annealed at 400 °C and 1 h: (a) standard tensile tests; (b) RHTTs.

Table 11
Parameters obtained from experimental RHTTs and yield strength estimation.

Material	Offset (mm)	P_y (N)	σ_y estimated (MPa)	Error (%)
Cu C12200 R360	0.340	89.10	319.1	−13.2
Cu C12200 R360 + Annealing	0.340	79.60	285.1	−0.02

4. Conclusions

The manufacturing process related to metallic tubular parts motivates that, in many cases, they show anisotropic mechanical properties. The standard testing procedures to characterize the yield strength are generally focused on the standard tensile test, but this is limited in these parts to longitudinal characterization. Taking into account that tubes and pipes are designed to support pressure loads, the most interesting testing direction is the hoop ones. This fact motivates the interest of researchers in the Ring Hoop Tension Test (RHTT) as an alternative mechanical characterization test for tubular parts. This investigation was focused on the applicability of an RHTT using simplified pins instead of D-shaped pins, in order to estimate the yield strength of metallic materials. After numerical FEM analyses and experimental tests, a novel RHTT was designed and the next conclusions were reached:

(a) Novelties for Small Ring Test:

(i) A correlation methodology for the estimation of the yield strength was designed based on the offset method of the standard tensile test.
(ii) From this numerical FEM analysis, the offset value with the lowest scattering was equal to 0.15 mm, and a correlation equation was obtained to relate the yield load P_y obtained from the SRT curve with the estimated yield strength σ_y. This correlation equation showed non-significant dependency with other mechanical properties (Young's modulus, proportional limit, hardening coefficient, or the presence of Lüders bands straining).

(b) Novelties for Ring Hoop Tension Test:

(i) The use of simplified pins instead of D-shaped pins motivated an important reduction in the dependency of the yield strength estimation with the frictional coefficient in the pin-ring contact.
(ii) The correlation methodology designed in the SRT, an offset method, was extended to other ring geometries with numerical FEM analyses and experimental tests, obtaining a correlation equation that took into account the influence of slenderness, thickness, and width of the ring.
(iii) Experimental tests on aluminum and copper pipes with different mechanical properties and ring geometries were performed in order to validate the previous equations and methodologies. The error level in the estimation of the yield strength in the case of the aluminum pipe was equal to 0.5%. The copper pipe, which was extremely cold-formed, showed an error of −13.2%. This error was related with the anisotropic behavior based on its cold-formed state. In order to verify this assumption, the copper pipe was annealed, obtaining a new yield strength estimation error of −0.02%. These results validated the

proposed correlation equations for the estimation of the yield strength of tubular parts in the hoop direction.

CRediT authorship contribution statement

Jose Calaf-Chica: Conceptualization, Methodology, Software, Writing – original draft, Investigation, Formal analysis, Writing – review & editing. **Jorge Martínez-Peña:** Investigation, Formal analysis, Writing – review & editing. **Pedro Miguel Bravo Díez:** Validation, Resources, Writing – review & editing, Supervision, Project administration. **Mónica Preciado Calzada:** Data curation, Investigation, Writing – review & editing.

Declaration of competing interest

The authors declare that they have no known competing financial interests or personal relationships that could have appeared to influence the work reported in this paper.

References

Aghamiri, S.M., Sowa, T., Ukai, S., Oono, N., Sakamoto, K., Yamashita, S., 2020. Microstructure and texture evolution and ring-tensile properties of recrystallized FeCrAl ODS cladding tubes. Mater. Sci. Eng. A 771, 138636.

ASM International, 2019. Properties and Selection of Aluminum Alloys. ASM International.

ASTM, 2021. ASTM E8 / E8M - 21 standard test methods for tension testing of metallic materials.

Baik, J.M., Kameda, J., Buck, O., 1983. Small punch test evaluation of intergranular embrittlement of an alloy steel. Scr. Metall. 17 (12), 1443–1447.

Calaf-Chica, J., Bravo Díez, P.M., Preciado Calzada, M., Garcia-Tarrago, M.J., 2020. Optimization of the t/10 offset correlation method to obtain the yield strength with the small punch test. J. Nuclear Mater. 534, 152177.

Daxner, T., Rammerstorfer, F.G., Fischer, F.D., 2005. Instability phenomena during the conical expansion of circular cylindrical shells. Comput. Methods Appl. Mech. Engrg. 194 (21–24), 2591–2603.

Dick, C.P., Korkolis, Y.P., 2014a. Assessment of anisotropy of extruded tubes by ring hoop tension test. Procedia Eng. 81, 2261–2266.

Dick, C.P., Korkolis, Y.P., 2014b. Mechanics and full-field deformation study of the Ring Hoop Tension Test. Int. J. Solids Struct. 51 (18), 3042–3057.

Garrison, B., Yan, Y., TerMaath, S., 2021. Determining failure properties of as-received and hydrided unirradiated Zircaloy-4 from ring compression tests. Eng. Fail. Anal. 125, 105362.

Gurovich, B.A., Frolov, A.S., Fedotov, I.V., 2020. Improved evaluation of ring tensile test ductility applied to neutron irradiated 42XNM tubes in the temperature range of (500–1100)° C. Nuclear Eng. Technol. 52 (6), 1213–1221.

Hiyoshi, N., Itoh, T., Sakane, M., Tsurui, T., Tsurui, M., Hisaka, C., 2020. Development of miniature cruciform specimen and testing machine for multiaxial creep investigation. Theor. Appl. Fract. Mech. 108, 102582.

ISO/IEC, 1998. ISO 8493:1998 - metallic materials — Tube — Drift-expanding test.

ISO/IEC, 2013a. ISO 8492:2013 - metallic materials — Tube — Flattening test.

ISO/IEC, 2013b. ISO 8494:2013 - metallic materials — Tube — Flanging test.

ISO/IEC, 2013c. ISO 8495:2013 - metallic materials — Tube — Ring-expanding test.

ISO/IEC, 2013d. ISO 8496:2013 - metallic materials — Tube — Ring tensile test.

ISO/IEC, 2019. ISO 6892-1:2019 - metallic materials — Tensile testing — Part 1: Method of test at room temperature.

Jiang, L., Jonas, J.J., Boyle, K., Martin, P., 2008. Deformation behavior of two Mg alloys during ring hoop tension testing. Mater. Sci. Eng. A 492 (1–2), 68–73.

Jiang, H., Wang, J.A.J., 2018. Development of cone-wedge-ring-expansion test to evaluate the tensile HOOP properties of nuclear fuel cladding. Prog. Nucl. Energy 108, 372–380.

Kazakeviciute, J., Rouse, J.P., De Focatiis, D.S., Hyde, C.J., 2019. The development of a novel technique for small ring specimen tensile testing. Theor. Appl. Fract. Mech. 99, 131–139.

Korkolis, Y.P., Kyriakides, S., Giagmouris, T., Lee, L.-H., 2010. Constitutive modeling and rupture predictions of Al-6061-T6 tubes under biaxial loading paths. J. Appl. Mech. 77 (6), 064501.

Ktari, Z., Leitão, C., Prates, P.A., Khalfallah, A., 2021. Mechanical design of ring tensile specimen via surrogate modelling for inverse material parameter identification. Mech. Mater. 153, 103673.

Kubík, P., Šebek, F., Petruška, J., Hůlka, J., Park, N., Huh, H., 2018. Comparative investigation of ductile fracture with 316L austenitic stainless steel in small punch tests: Experiments and simulations. Theor. Appl. Fract. Mech. 98, 186–198.

Kuwabara, T., Sugawara, F., 2013. Multiaxial tube expansion test method for measurement of sheet metal deformation behavior under biaxial tension for a large strain range. Int. J. Plast. 45, 103–118.

Lee, J.M., Hwang, J.H., Kim, Y.J., Kim, J.W., 2021. Predicting ductile fracture of cracked pipes using small punch test data. Eur. J. Mech. A Solids 87, 104211.

Manahan, M.P., Argon, A.S., Harling, O.K., 1981. The development of a miniaturized disk bend test for the determination of postirradiation mechanical properties. J. Nuclear Mater. 104 (C), 1545–1550.

Nazari Tiji, S.A., Park, T., Asgharzadeh, A., Kim, H., Athale, M., Kim, J.H., Pourboghrat, F., 2020. Characterization of yield stress surface and strain-rate potential for tubular materials using multiaxial tube expansion test method. Int. J. Plast. 133, 102838.

Nozaki, M., Sakane, M., Fujiwara, M., 2020. Low cycle fatigue testing using miniature specimens. Int. J. Fatigue 137, 105636.

Rouse, J.P., Simonelli, M., Hyde, C.J., 2020. On the use of small ring testing for the characterisation of elastic and yield material property variation in additively manufactured materials. Addit. Manuf. 36, 101589.

Simonovski, I., Baraldi, D., Holmström, S., Altstadt, E., Delville, R., Bruchhausen, M., 2018. Determining the ultimate tensile strength of fuel cladding tubes by small punch testing. J. Nuclear Mater. 509, 620–630.

Tantideeravit, S., Kamaya, M., 2020. An application of FEM in the determination of tensile properties for work-hardened carbon steel by means of small punch test. Results Mater. 8, 100142.

Zheng, P., Chen, R., Liu, H., Chen, J., Zhang, Z., Liu, X., Shen, Y., 2020. On the standards and practices for miniaturized tensile test – A review. Fusion Eng. Des. 161, 112006.

Zhong, J., Song, M., Guan, K., Dymacek, P., 2020. Application of a database in the evaluation of strengths of Cr-Mo steels by means of small punch test. Int. J. Mech. Sci. 166, 105195.